Acta Scientiarum

http://periodicos.uem.br/ojs
ISSN on-line: 1807-8664
Doi: 10.4025/actascitechnol.v46i1.69552

Influence of Water Concentration on the Water/Vapor/ Oil Separation Process in a Vacuum Oil Filter: Modelling and Simulation

Chen Bin[1] and Liu Ge[2*]

[1]School of Mechanical & Electrical, Hebei Key Laboratory of Safety Monitoring of Mining Equipment, North China Institute of Science and Technology, Hebei, China. [2]School of Environmental Engineering, Hebei Key Laboratory of Hazardous Chemicals Safety and Control Technology, North China Institute of Science and Technology, Hebei, 065201, China. *Author for correspondence. E-mail: lycy@ncist.edu.cn

ABSTRACT. The vacuum oil filter (VOF) is widely applied in the oil-water emulsion demulsification separation due to the phase separation by using vacuum evaporation; however, the micro-dynamic characteristics of oil, water and vapor three phases and the influencing factors of separation efficiency are rarely studied. Therefore, the fluid flow and phase separation characteristics of water-in-oil emulsions were numerically analysed by ANSYS software. The demulsification conditions of water/oil emulsion were simulated by using the two-fluid model and the water evaporation model, and the turbulence effect was considered by using the Reynolds stress model. The results show that the established model could provide a convenient way to study the effects of the different water concentrations in oil; the turbulence intensity in VOF increases with the increase of water concentration in oil; The separation efficiency has been influenced by the inlet water concentration reaching values between 20.65-22.62% in the center axis, while 33.18-42.24% in the plate column; the vapor concentration ranged from 0 - 23.64% in the center axis, while 0 - 41.02% in the plate column. The relative volume fraction of water concentration decay tending with the water concentration increases, and the water concentration has a great influence on the separation efficiency.

Keywords: water evaporation model; separation efficiency; the vacuum oil filter; water concentration; water-in-oil emulsion.

Received on September 10, 2023.
Accepted on March 05, 2024.

Introduction

According to World Energy Outlook (International Energy Agency [IEA], 2021), global oil demand will increase by 5.7 million barrels to 96.7 million barrels a day in 2021 compared with 2020, thanks to the spread of more efficient cars and electric vehicles. So, the world economy will become much more dependent on oil. In many cases, pollutants such as water, sand, rust, dust, catalyst powder, and other solid particles are present in the oil during use, and caused by thermal degradation of the oil by unstable oil, degradation products, metal fragments, and other suspended solids, resulting in the loss of its function after the oil performance reaches a critical threshold (Bin & Ge, 2022). Thereby, the reuse of energy is the cheapest and most effective way to reduce energy demand.

The oil-water emulsion is a common by-product in the production process, usually, more than 90% of the emulsion could be reused by some demulsification methods, it is necessary to promote the phase separation to reduce oil energy demand; so, the efficient removal of the dispersed water phase from the continuous oil phase is one of the research hotspots at present. Currently available oil-water demulsification methods include chemical demulsification, gravity or centrifugal sedimentation, filtration, heat treatment, and membrane separation (Wang et al., 2021), etc. Among them, chemical demulsification has a unicity treatment for a certain water/oil emulsion, there is no universality of treatment; centrifugal separation is more effective for emulsions with large water content in oil; heat treatment can reduce the viscosity of oil, so that any water droplets can drop through the oil phase more quickly and help to separate water from oil, but higher oil temperature easily causes oil degradation; Membrane separation can be used to remove most of the water in the emulsion, thus reducing the volume of water(Abdulredha, Siti Aslina, & Luqman, 2020; Clint, Fletcher, & Todorov, 1999). However, such methods as heat treatment, chemical treatment, and membrane separation have high treatment costs

and complex operations. Especially, the chemical demulsification method may cause secondary contamination when removing the demulsifies from the water phase and oil phase.

In order to improve the demulsification efficiency of a water-in-oil emulsion, the researchers proposed some combination of treatment methods, such as emulsion demulsification method combined with the unstable settlement, filtration and vacuum evaporation, etc. (Gutiérrez, Lobo, Benito, Coca, & Pazos, 2011; Wang et al., 2021). Where, vacuum evaporation is a common wastewater/oil emulsion treatment technology in industrial, which can produce efficient dehydration effect at appropriate emulsion temperature; the filtration or sedimentation treatment of water/oil emulsion can remove the particulate pollutants from the oil/water emulsion before the vacuum evaporation treatment, to improve the dehydration effect of vacuum evaporation by experiment verification.

A vacuum oil filter (VOF) is a specific application of the water/oil separation synthesis method and consists of a cylindrical section with a fan-shaped baffle and a plate column connected to a central section. The columnar section is the separation chamber of the water-in-oil emulsion. The upper half of the cylinder is provided with an inlet pipe and a vapor discharge pipe (i.e., the vacuum outlet) respectively, and the lower half of the cylinder is provided with an oil discharge pipe, as shown in Figure 1.

The vacuum outlet relates to the vacuum pump to provide a certain vacuum inside the VOF. Under the action of standard atmospheric pressure, the oil-water emulsion with a certain temperature is ejected in from the inlet pipe on the top of the VOF through the fan-shaped baffles into the circular tank body; Multilayer corrugated orifice is arranged in the middle of the tank body, so the emulsion has a zigzag and complicated path in the orifice, and the water in the oil is fully evaporated. The vapor is discharged from the tank body upward through the vacuum outlet. The VOF involves three kinds of fluids: oil, water, and vapor, which is a complex separation system of mass transfer and phase transition coupling.

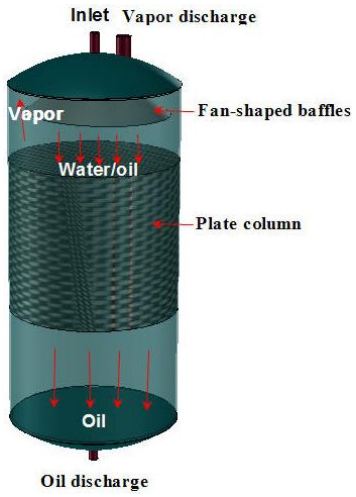

Figure 1. Schematic of vacuum oil filter

Many investigations have been performed in the literature related to describing and improving the water/oil separation process using vacuum evaporation, such as the patent on vacuum distillation system was published by Cellini, Ronghi, and Geren, (1988), disclosed for purifying contaminated liquids, i.e. seawater, brackish water, and chemical effluents; a range of papers have been published concerning the operation of vacuum evaporation, as well as some mathematical models describing velocity profiles, the pressure drop, and the separation efficiency(Abdulredha et al., 2020; Gong, Li, Zhang, Peng, Yu, & Mou, 2021; Laza-Knoerr, Huang, Grossiord, Couvreur, & Gref, 2011). Haelssig, Tremblay, Thibault, and Etemad, (2010) presents a direct numerical simulation method for the interfacial dynamics of multicomponent systems and fluid volume for simultaneous interfacial heat and mass transfer, the method incorporates the full interface species and energy jump conditions for vapor-liquid interphase heat and mass transfer, thus, making it applicable to systems with multiple phases changing species to many industrially important applications, were coupled interphase heat and mass transfer occur, including distillation. Abu-Zaid (2004) carried out systematic and detailed experiments and obtained the variation of the evaporation time of kerosene and diesel emulsion on stainless steel and aluminium with surface temperature. However, the micro-dynamic characteristics of oil, water, and vapor three phases in the process of vacuum evaporation and the influencing factors of separation efficiency are rarely studied.

Computational Fluid Dynamics (CFD) provides a way to predict a wide range of design and operating conditions under a velocity profile, it operates on simple laws such as the laws of thermodynamics, momentum, energy, and Euler's equations. The numerical treatment of the Navier–Stokes equation ensuing from these laws is what governs fluid dynamics. CFD is more suited to steady-state flow which is less demanding for the computer and enables the solutions to be achieved within a reasonable number of iterations. This resulted from the rapid improvement in computers and a better understanding of the numerical treatment of turbulence. As such it offers a means of testing theoretical advances for conditions unavailable experimentally (Fletcher, 1988; Zhao et al., 2020). Therefore, the aim of this study was to analyze numerically by CFD the fluid flow and phase separation characteristics of oil-in-water emulsions, using the two-fluid model and the water evaporation model, and the turbulence effect was considered by using the Reynolds stress model.

Therefore, the outline of the rest of this paper is as follows. In Section 2, the modelling was established to study the influence of water concentration by using the two-fluid model and the water evaporation model, and the Reynolds stress model; the simulations were carried out on the VOF. In Section 3, the streamline, volume fraction, and separation efficiency of VOF were analyzed, and the influence of water phase concentration on the oil-water separation process was obtained. Finally, we conclude in Section 4.

Material and Methods

I Mathematical model

In the implementation of oil-water emulsion dehydration in VOF, emulsion descends flow in the VOF tank through the import into the tank top by gravity flow down, as a result of the plate column block make its flow path to extend and residence time increases, the water in oil is part of the evaporation; the oil after dehydration drains out of the tank through the oil drain at the bottom of the tank. The vapor phase is formed by the evaporation of water in the oil that accumulates in the tank upstream in the vapor discharge pipe through the action of a vacuum pump. The process of VOF dehydration is the simultaneous heat and mass transfer between vapor and water. Obviously, the efficiency of heat and mass transfer is directly related to the flow pattern of the fluid in the system, which largely depends on the interface area through which heat and mass are transferred. If the VOF is assumed to operate under transient conditions in which classical fluid dynamics equations can be applied, the mathematical model describing the flow of water/vapor/oil multiphase fluids within the VOF consists of two sets of conservation equations: the mass balance of each phase and the momentum balance, this is, the dynamic characteristics of each phase in the multiphase flow field of VOF can be determined by using the continuity equation and momentum equation, and the mathematical model of VOF is established as follows.

(1) The continuity equation

In this case, the oil phase was specified as the primary phase and thus the volume fraction of the oil phase was solved. It follows that a computational cell is filled with oil when the volume fraction is unity, filled with water when the volume fraction is zero, and partially filled with oil when the volume fraction is between zero and one. The continuity equation takes the following form,

$$\frac{\partial\left(f_i\rho_i\right)}{\partial t}+\frac{\partial\left(f_i\rho_i u_i\right)}{\partial x}+\frac{\partial\left(f_i\rho_i v_i\right)}{\partial y}+\frac{\partial\left(f_i\rho_i w_i\right)}{\partial z}=S_m \tag{1}$$

Where, the subscript i represent the phases involved (water, oil, and vapor); f_i is the volume fraction of the i phase; ρ_i is density of the i phase, and u_i, v_i, w_i is the velocity of the i phase in x, y, z direction, respectively; S_m describes the mass flow rate per unit volume from the water phase to vapor phase, which occurs if the interphase mass transfer takes place.

(2) The momentum equation

By the Navier-Stokes equations for incompressible flows along with the appropriate model are adopted in the VOF, the momentum conservation equation is given by,

$$\begin{aligned}
&\frac{\partial(f_i\rho_i u_i)}{\partial t}+u_i\frac{\partial(f_i\rho_i u_i)}{\partial x}+v_i\frac{\partial(f_i\rho_i u_i)}{\partial y}+w_i\frac{\partial(f_i\rho_i u_i)}{\partial z}=\rho_i g_x-\frac{\partial(f_i p_i)}{\partial x}+\mu_i\left(\frac{\partial^2(f_i u_i)}{\partial x^2}+\frac{\partial^2(f_i u_i)}{\partial y^2}+\frac{\partial^2(f_i u_i)}{\partial z^2}\right)+\Psi_{\alpha\beta x}+F_x\\
&\frac{\partial(f_i\rho_i v_i)}{\partial t}+u_i\frac{\partial(f_i\rho_i v_i)}{\partial x}+v_i\frac{\partial(f_i\rho_i v_i)}{\partial y}+w_i\frac{\partial(f_i\rho_i v_i)}{\partial z}=\rho_i g_y-\frac{\partial(f_i p_i)}{\partial y}+\mu_i\left(\frac{\partial^2(f_i v_i)}{\partial x^2}+\frac{\partial^2(f_i v_i)}{\partial y^2}+\frac{\partial^2(f_i v_i)}{\partial z^2}\right)+\Psi_{\alpha\beta y}+F_y\\
&\frac{\partial(f_i\rho_i w_i)}{\partial t}+u_i\frac{\partial(f_i\rho_i w_i)}{\partial x}+v_i\frac{\partial(f_i\rho_i w_i)}{\partial y}+w_i\frac{\partial(f_i\rho_i w_i)}{\partial z}=\rho_i g_z-\frac{\partial(f_i p_i)}{\partial z}+\mu_i\left(\frac{\partial^2(f_i w_i)}{\partial x^2}+\frac{\partial^2(f_i w_i)}{\partial y^2}+\frac{\partial^2(f_i w_i)}{\partial z^2}\right)+\Psi_{\alpha\beta z}+F_z
\end{aligned} \tag{2}$$

Where μ_i is the dynamic viscosity of the i phase; p_i is the pressure of the i phase; g_x, g_y, g_z describes the gravitational body force in x, y, z direction, respectively; $\Psi_{\alpha\beta x}$, $\Psi_{\alpha\beta y}$, $\Psi_{\alpha\beta z}$ represents momentum transfer induced by interphase mass transfer and occurs when mass is carried from αphase into βphase in x, y, z direction, respectively; F_x, F_y, F_z describes the total force on one phase due to interaction with other phases, such as drag force, lift force, virtual mass force, etc. in this case, includes forces due to surface tension. Employing the Continuum Surface Force (CSF) model proposed by Brackbill, Kothe, and Zemach, (1992), the surface tension force is calculated by the following equation,

$$F=\sigma\frac{\rho\bar{\kappa}\nabla f_o}{0.5(\rho_o+\rho_w)} \tag{3}$$

where f_o is the volume fraction of the oil phase. σ, ρ_o, ρ_w, and $\bar{\kappa}$ are the water/oil surface tension, oil density, water density and curvature, respectively. ρ is the water/oil mixture density, $\rho=f_o\rho_o+(1-\rho_o)\rho_w$. The curvature is determined from the unit normal vector according to the following equation, $\bar{\kappa}=-(\nabla\cdot\hat{n})$, where the unit normal vector is $\hat{n}=\frac{\nabla f_o}{|\nabla f_o|}$, which points from the water to the oil phase.

(3) The Reynolds Stress Model

The movement of the oil and water within the VOF is very complex and has turbulent characteristic. So, to describe the multiphase flow inside the VOF correctly, it is necessary to use an appropriate turbulent model.

The time-averaged equations are obtained by decomposing each flow variable into a mean and fluctuating part. There is an unclosed term that arises in the time-averaged momentum equation (Eq.2), which are the Reynolds stress tensor $\frac{\partial}{\partial x}\left(f_i\rho_i\overline{u_i'v_i'}\right)$, $\frac{\partial}{\partial y}\left(f_i\rho_i\overline{u_i'v_i'}\right)$, $\frac{\partial}{\partial x}\left(f_i\rho_i\overline{u_i'w_i'}\right)$, $\frac{\partial}{\partial z}\left(f_i\rho_i\overline{u_i'w_i'}\right)$, $\frac{\partial}{\partial y}\left(f_i\rho_i\overline{w_i'v_i'}\right)$, $\frac{\partial}{\partial z}\left(f_i\rho_i\overline{w_i'v_i'}\right)$, $\frac{\partial}{\partial x}\left(f_i\rho_i\overline{u_i'u_i'}\right)$, $\frac{\partial}{\partial y}\left(f_i\rho_i\overline{v_i'v_i'}\right)$, $\frac{\partial}{\partial z}\left(f_i\rho_i\overline{w_i'w_i'}\right)$, the most common closures used for the Reynolds stress tensor are linear models based on the Boussinesq approximation. The Reynolds stress model involves a calculation of the individual Reynolds stresses, using differential transport equations, which may be written as follows:

$$\begin{aligned}
&\frac{\partial}{\partial t}\left(f_i\rho_i\overline{u_i'v_i'}\right)+\frac{\partial}{\partial z}\left(f_i\rho_i w_i\overline{u_i'v_i'}\right)=-\frac{\partial}{\partial z}\left[f_i\rho_i\overline{u_i'v_i'w_i'}+\overline{p_i\left(\delta_{zy}u_i'+\delta_{zx}v_i'\right)}\right]\\
&+\frac{\partial}{\partial z}\left[\mu_i\frac{\partial}{\partial z}\left(f_i\overline{u_i'v_i'}\right)\right]-f_i\rho_i\left(\overline{u_i'w_i'}\frac{\partial v_i}{\partial z}+\overline{v_i'w_i'}\frac{\partial u_i}{\partial z}\right)-f_i\rho_i\left(g_x\overline{v_i'\theta}+g_y\overline{u_i'\theta}\right)\\
&+\overline{p_i\left(\frac{\partial u_i'}{\partial y}+\frac{\partial v_i'}{\partial x}\right)}-2\mu_i\overline{\frac{\partial u_i'}{\partial z}\frac{\partial v_i'}{\partial z}}-2\rho_i\Omega_z\left(\overline{v_i'q_i'}\,\varepsilon_{xzm}+\overline{u_i'q_i'}\,\varepsilon_{yzm}\right)
\end{aligned} \tag{4}$$

where $\overline{u_i'}, \overline{v_i'}, \overline{w_i'}$ is the velocity fluctuation average of the i phase in x, y, z direction, respectively; the terms are local time derivative, convection, turbulent diffusion, molecular diffusion, stress production, buoyancy

production, pressure strain, dissipation, and production by system rotation, respectively. The turbulent diffusion has been simplified in ANASYS FLUENT to use a scalar turbulent diffusivity as follows,

$$-\frac{\partial}{\partial z}\left[f_i\rho_i\,\overline{u_i'v_i'w_i'} + \overline{p_i\left(\delta_{zy}u_i' + \delta_{zx}v_i'\right)}\right] \approx \frac{\partial}{\partial z}\left(\frac{\mu_{it}}{\sigma_z}\,\overline{\frac{\partial u_i'v_i'}{\partial z}}\right) \tag{5}$$

Where, $\sigma_z = 0.82$, μ_{it} is the turbulent viscosity, which is computed using equation $\mu_{it} = \rho C_\mu \frac{\kappa^2}{\varepsilon}$. ε is the turbulence eddy dissipation, κ is the turbulent kinetic energy, $C_\mu = 0.09$ .When turbulence dissipation appears in the individual stress equations, an equation for ε is still required. It has now the form,

$$\begin{aligned}&\frac{\partial(\rho_i\varepsilon)}{\partial t} + \frac{\partial(\rho_i\varepsilon u_i)}{\partial x} + \frac{\partial(\rho_i\varepsilon v_i)}{\partial y} + \frac{\partial(\rho_i\varepsilon w_i)}{\partial z} = \frac{\partial}{\partial x}\left[\left(\mu_i + \frac{\mu_{it}}{\sigma_\varepsilon}\right)\frac{\partial\varepsilon}{\partial x}\right] + \\ &\frac{\partial}{\partial y}\left[\left(\mu_i + \frac{\mu_{it}}{\sigma_\varepsilon}\right)\frac{\partial\varepsilon}{\partial y}\right] + \frac{\partial}{\partial z}\left[\left(\mu_i + \frac{\mu_{it}}{\sigma_\varepsilon}\right)\frac{\partial\varepsilon}{\partial z}\right] + C_{\varepsilon 1}\frac{\varepsilon\left(P_{xx} + C_{\varepsilon 3}G_{xx}\right)}{2\kappa} - C_{\varepsilon 2}\rho_i\frac{\varepsilon^2}{\kappa}\end{aligned} \tag{6}$$

Where P_{xx} and G_{xx} are defined as stress production, buoyancy production; $C_{\varepsilon 1}, C_{\varepsilon 2}$ and $C_{\varepsilon 3}$ are Reynold's stress model constants.

One of the most important terms in the Reynolds stress model is the pressure-strain correlation, φ. This model has been demonstrated to give superior performance in a range of basic shear flows, including plane strain, rotating plane shear, and axisymmetric expansion/contraction. The pressure-strain correlations can be expressed in the general form as follows:

$$\begin{aligned}&\phi_{xy} = -\left(C_1\rho_i\varepsilon + C_1^* P\right)b_{xy} + C_2\rho_i\varepsilon\left(b_{xz}b_{yz} - \frac{1}{3}b_{mn}b_{mn}\delta_{xy}\right) + \left(C_3 - C_3^*\sqrt{b_{xy}b_{xy}}\right)\rho_i\kappa S_{xy} \\ &+C_4\rho_i\kappa\left(b_{xz}S_{yz} + b_{yz}S_{xz} - \frac{2}{3}b_{mn}S_{mn}\delta_{xy}\right) + C_5\rho_i\kappa\left(b_{xz}\Omega_{yz} + b_{yz}b_{mn}\Omega_{xz}\right)\end{aligned} \tag{7}$$

where, b_{xy} is the Reynolds-stress anisotropy tensor defined as $b_{xy} = -\frac{-\rho_i\,\overline{u_i'v_i'} + \frac{2}{3}\rho_i\kappa\delta_{xy}}{2\rho_i\kappa}$; the mean strain rate, S_{xy} , is defined as $S_{xy} = \frac{1}{2}\left(\frac{\partial v_i}{\partial x} + \frac{\partial u_i}{\partial y}\right)$; the mean rate-of-rotation tensor, Ω_{xz} , is defined by $\Omega_{xz} = \frac{1}{2}\left(\frac{\partial u_i}{\partial y} - \frac{\partial v_i}{\partial x}\right)$; the constants are $C_1 = 3.4, C_1^* = 1.8, C_2 = 4.2, C_3 = 0.8, C_3^* = 1.3, C_4 = 1.25, C_5 = 0.4$

(4) Water Evaporation Model

Consider the case of VOF in which the dispersed water phase is in the form of discrete single-component spherical water droplets with a density much larger than that of the surrounding ambient oil at a temperature T_∞, interactions of the oil with only one single drop, it can be assumed that the total heat capacity of the oil much larger than that of the water and T_∞, far from the drop surface, is constant; and momentum exchange with the carrier oil is assumed to be only a function of the drag force (i.e. Basset history, added mass and other terms are neglected). Furthermore, the thermal energy exchange between phases is assumed to occur only through convective heat transfer, and internal droplet vortical flow is neglected. If both the water and the oil are incompressible with constant properties, thus the conservation equation for energy is described as,

$$\frac{\partial T_i}{\partial t} + u_i\frac{\partial T_i}{\partial x} + v_i\frac{\partial T_i}{\partial y} + w_i\frac{\partial T_i}{\partial z} = \frac{\lambda_i}{\rho_i c_i}\left(\frac{\partial^2 T_i}{\partial x^2} + \frac{\partial^2 T_i}{\partial y^2} + \frac{\partial^2 T_i}{\partial z^2}\right) \tag{8}$$

where, the subscript i denote the phases in the VOF, i.e., water droplet (w), oil phase (o), vapor phase of the evaporate (v); λ_i and c_i are the liquid thermal conductivity coefficient and specific heat capacity respectively; T_i is the droplet temperature.

II Description and geometry of the simulated VOF

The tank of the simulated VOF is 1.1 m high, with a radius of 0.225 m cylinders, a porous medium is 0.4m high located at 0.35 m from the inlet. Two outlets are positioned at the top and bottom of the separation chamber to separate vapor and oil respectively. Due to symmetry, only half the separation chamber is modelled using ANSYS software, for complex geometries, quad/ hex meshes show no numerical advantage, and meshing effort can be saved by using a Tri/ Tetrahedral mesh. Since the separation chamber has a complex geometry, a Tri/ Tetrahedral mesh was used with an interval size of 0.12 m. The VOF used in the numerical simulation work is shown in Figure 1.

(1) Meshing scheme

The present computational model is based on the 3D geometric model, the triangular mesh is used to mesh the interface between the inlet and the separation cavity. A boundary layer mesh is generated in the wall near the combustion chamber by using a tetrahedral unstructured mesh. To capture the low-pressure central region, a block-structured grid is generated in this region. In addition, a grid is generated near the inlet area where the maximum expansion ratio is limited to about 10, which is important for capturing backflow through the steam discharge tube opening. Grid independence was studied under 5 different grid densities ranging from 750,000 to 2 million. The study of water distribution shows that better prediction can be obtained under higher mesh density. The entire grid was generated using Gambit 2.3.16. Figure 2 shows the grid on the VOF with 312,057 cells, which is considered the best choice for good prediction and reasonable simulation time.

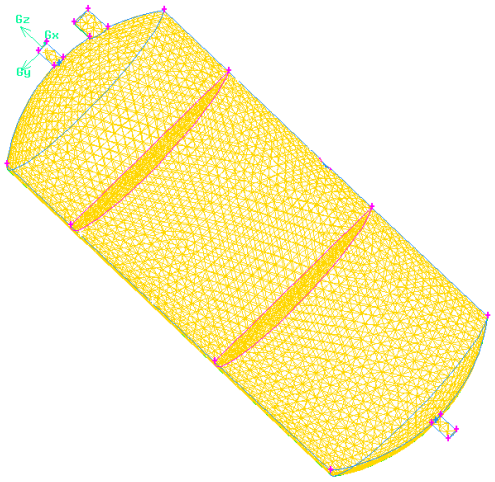

Figure 2. The unstructured mesh used in the CFD calculations.

(2) Simulation

It is assumed that the simulation of VOF is carried out under the action of water and oil, and the numerical simulation adopts the Cartesian coordinate system shown in Figure 2. The multi-phase flow simulation under the transient and turbulent states is carried out with a 3D double-precision flow field. The governing equations are solved in turn (that is, isolated from each other), since the governing equation is nonlinear (and coupled), several iterations must be performed in the solution cycle to obtain a convergent solution.

The boundary conditions prescribed by the inlet pressure (101.3 kPa) are applied at the entrance of the VOF; For vapor and oil discharges, we use the prescribed outlet pressures (2kPa and 101.3kPa) boundary conditions; The volume fraction of feed steam was set as zero, and volume fractions of feed water were 0.01, 0.05, 0.10, 0.15 and 0.20 respectively. The first physical constant of the liquid is set as the physical constant of the oil, the second physical constant of the water, and the third physical constant of the steam.

Based on its good stability, which is suitable for general CFD computing, the IMPLICIT computing scheme is adopted. A PRESTO pressure interpolation scheme is used, which is very suitable for the steep pressure

gradient involved in a vortex flow. The first-order windward difference discriminant scheme is selected for momentum, volume fraction, turbulent kinetic energy, and turbulent dissipation rate. The Reynolds stress model (RSM) was used to independently evaluate and compare the simulation results. A SIMPLE algorithm is applied to pressure-velocity coupling. The high order quadratic windward interpolation (QUICK) spatial resolution scheme was chosen for the interpolation of field variables from the cell canter to the control surface because it was reported to be useful for vortex flows. Approximately 6000 incremental steps were performed in the simulation, and the default value of the general convergence standard 1×10^{-6} was implemented.

Results and discussion

I Effect of streamline distribution on the separation process

To illustrate the numerical simulation results of the approach described in section 2, the streamline distribution of oil, water, and vapor phase with different water volumetric fractions in the inlet section on the separation process is shown in Figure 3, 4, and 5, respectively. By analysing the figures we can observe that with increasing the water concentration (or volume fraction) in oil, the turbulent intensity of the oil phase decreases (Figure 3), simultaneously that of the water phase increases (show in Figure 4), that of vapor phase are practically independents of inlet water concentration of the mixture (Figure 5); and that the streamline of oil, water and vapor phase is divided into three layers by the plate column in the centre of the VOF, the velocity of the oil and water in the middle layer is slowly, and the volume fraction of the oil and water in that layer is small compared to other two layers, when they migrate through the plate column to the bottom of the VOF; moreover, the streamlines for vapor has been opposite in Figure 5, this is the volume fraction in the middle layer is greater than upper and bottom layer, despite the middle layer velocity is also slowly. This behaviour can be explained basically that the oil and water phase had a tortuous path due to the external and internal fields of acceleration (gravity and drag forces) and by the exerted flow resistance by the plate column. However, the water or oil phase in the middle layer migrates slowly through the plate column not only enhancing the unit productive rate, but also improving the effective vaporization acreage, to prevent them from passing through the separation chamber quickly adequate extending an evaporation period. Features of these streamline distributions such as the separate section flow and vortex are factors contributing to the evaporate effectiveness of the VOF. By increasing the water concentration into the VOF, we have greater turbulent intensity between water and vapor to improve the water/oil phase separation.

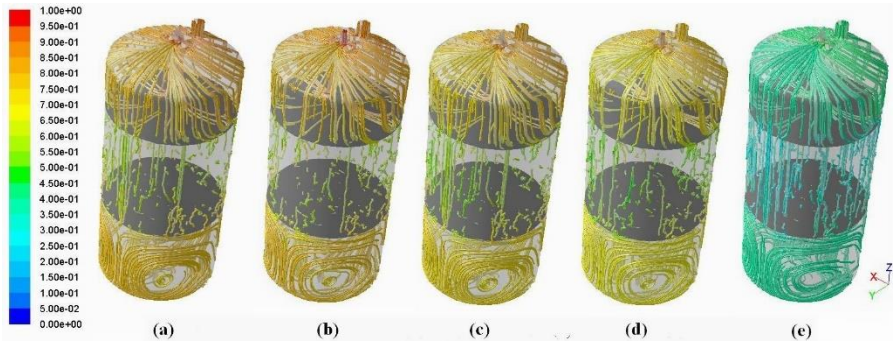

Figure 3. Streamlines of oil phase to different inlet water volumetric fraction: (a) 0.005; (b) 0.01; (c) 0.05; (d) 0.10; (e) 0.50.

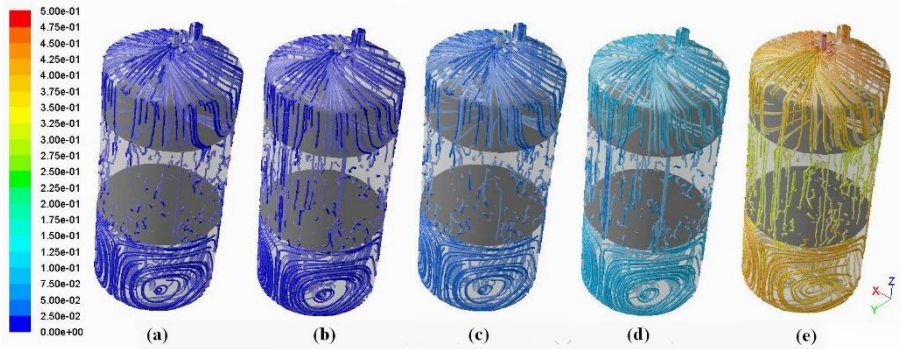

Figure 4. Streamlines of water phase to different inlet water volumetric fraction: (a) 0.005; (b) 0.01; (c) 0.05; (d) 0.10; (e) 0.50.

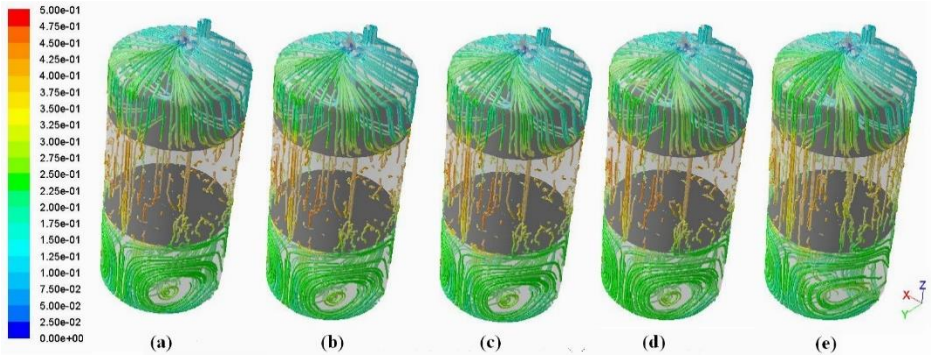

Figure 5. Streamlines of vapor phase to different inlet water volumetric fraction: (a) 0.005; (b) 0.01; (c) 0.05; (d) 0.10; (e) 0.50.

II Effect of volume fraction on the separation process

The effects of the different volume fractions of oil, water, and vapor phase on the separation process in VOF were analyzed, Figure 6-7 shows the oil and vapor concentration distribution fields in the yz plane for x = 0 and xy plane for z = -293, -693, respectively. From the contours of oil and vapor concentration distribution fields in Figure 6-7, it can be observed that there is a higher distribution of water concentration near the wall of the VOF. This is, the concentration distribution near the VOF wall of the water phase in the separation zone is largely due to water-dense is larger compared to that of the oil phase and is evaporated; the less dense of oil phase accumulates in the middle of the separation column and gradually settles to the bottom of the separation chamber.

The red colour according to the contour line indicates maximum oil concentration, while blue indicates maximum water concentration in Figure 6, it shows that with inlet water volumetric fraction increase, the level of oil concentration decreased gradually along with redial and axial directions, and decay quickly in the plate column section. However, when the water concentration is increased to 0.50 as shown in Figure 6(e), the level of oil concentration in the plate column has decreased slower than in other cases; this is consistent with the distribution of the relative volume fraction of oil phase on the canter axis of inlet and outlet of VOF as shown in Figure 8, resulting in water in oil is evaporated incompletely. This situation can be seen in Figure 7, which depicts the distribution of vapor concentration is lower on the yz plane and xy plane.

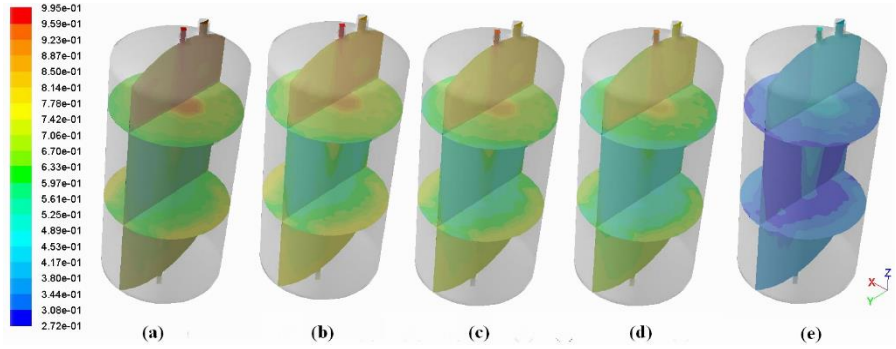

Figure 6. Oil fields in the yz plane for x = 0 and xy plane for z=-293, -693 with different water volumetric fraction: (a) 0.005; (b) 0.01; (c) 0.05; (d) 0.10; (e) 0.50.

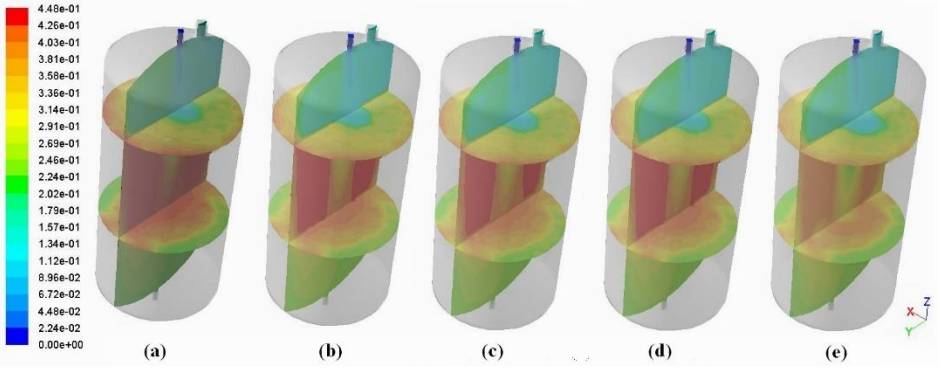

Figure 7. Vapor fields in the yz plane for x = 0 and xy plane for z=-293, -693 with different water volumetric fraction: (a) 0.005; (b) 0.01; (c) 0.05; (d) 0.10; (e) 0.50.

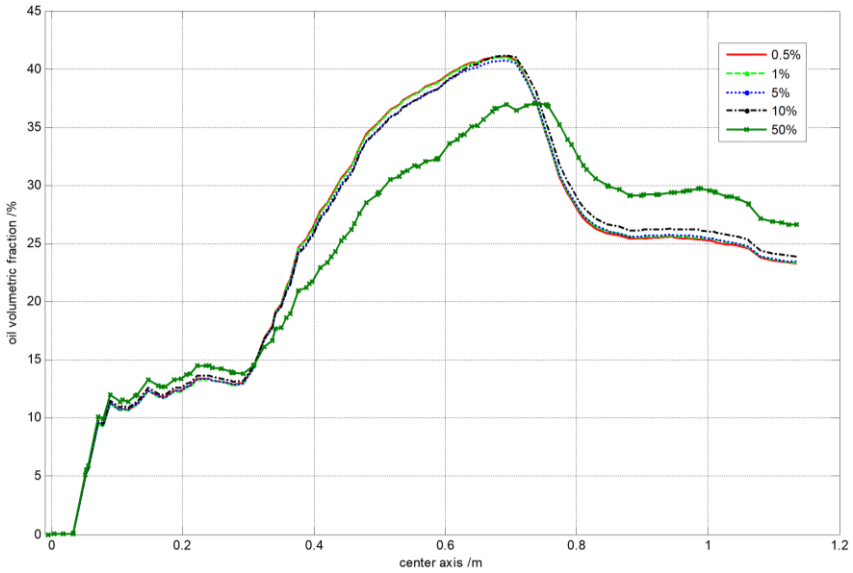

Figure 8. the distribution of relative volume fraction of oil phase on the center axis.

According to the distribution of the volume fraction of the oil phase along the central axis in Figure 8, the volume fraction of the oil phase on the separation column plate (the corresponding central axis is within the range of 0.5-0.9m) is significantly larger, indicating that there is less water in the oil in this region, and the separation of oil and water is realized, that is, the separation column plate of VOF plays an important role in the separation effect.

It can be seen from Figure 7 that the distribution of the vapor phase concentration by water evaporated in the oil is also large in the separation column plate, and there is a ring region with a large evaporation effect in the radial direction; with the increase of water content in oil, the vapor phase concentration decreases gradually.

In summary, as the results showed that with the increase of water concentration results in a decrease in oil concentration in the plate column section, thereby it brings any water into the bottom of the separator, so the evaporation efficiency decays. Thus, the design of the separator should take cognizance of the water concentration in oil such that when the water concentration is high, the geometry of the separator can be changed by increasing the plate column height.

III Separation efficiency

An increase in water content from 0.5 to 50% is seen to affect the separation efficiency of the VOF, the separation efficiency can be calculated by the following equations,

$$E_{separation} = \frac{V_{inlet} - V_{outlet}}{V_{inlet}} \times 100\% \tag{9}$$

Where V_{inlet} and V_{outlet} are inlet and outlet volumetric fraction of water.

Figure 9-10 are the distribution of the relative volume fraction of the water phase and vapor phase on the centre axis of the inlet and outlet of the VOF, respectively. Figure 9 illustrates that the separation efficiency has been influenced by the inlet water concentration reaching values between 20.65-22.62 % in the canter axis, while 33.18-42.24% in the plate column. The relative volume fraction of water concentration decay tending with the water concentration increases.

Figure 10 shows that the vapor concentration ranged from 0 - 23.64% in the centre axis, while 0 - 41.02% in the plate column. When the water content in the oil reaches 50%, the maximum volume fraction of the vapor phase in the separation column plate is 0.35%, while when the content is less than 50%, the maximum difference of the volume fraction of the vapor phase is not large. When the water content in the oil is around 50% (i.e., the critical point of an inverse phase of the water-in-oil emulsion), the separation efficiency of VOF will drop sharply. However, under the condition of different water content in oil, the vapor phase volume fraction at the VOF outlet is basically unchanged.

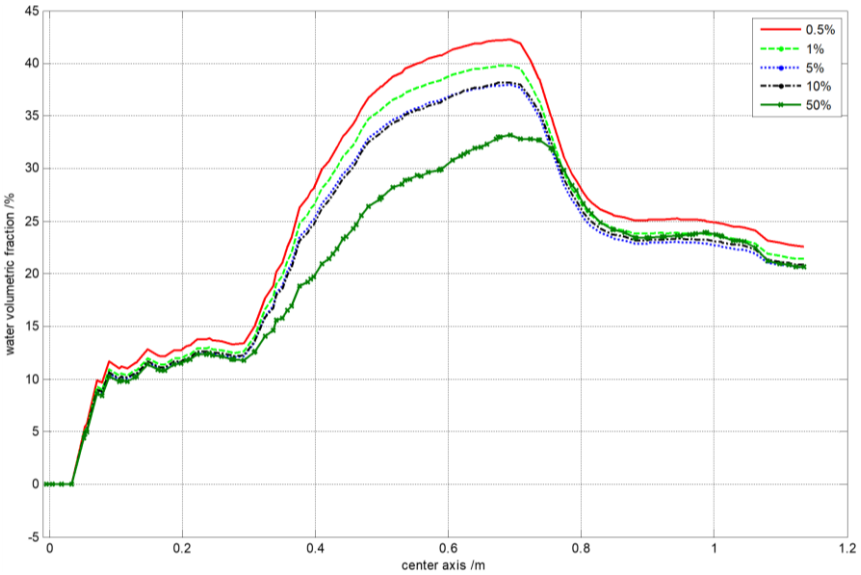

Figure 9. the distribution of relative volume fraction of water phase on the center axis.

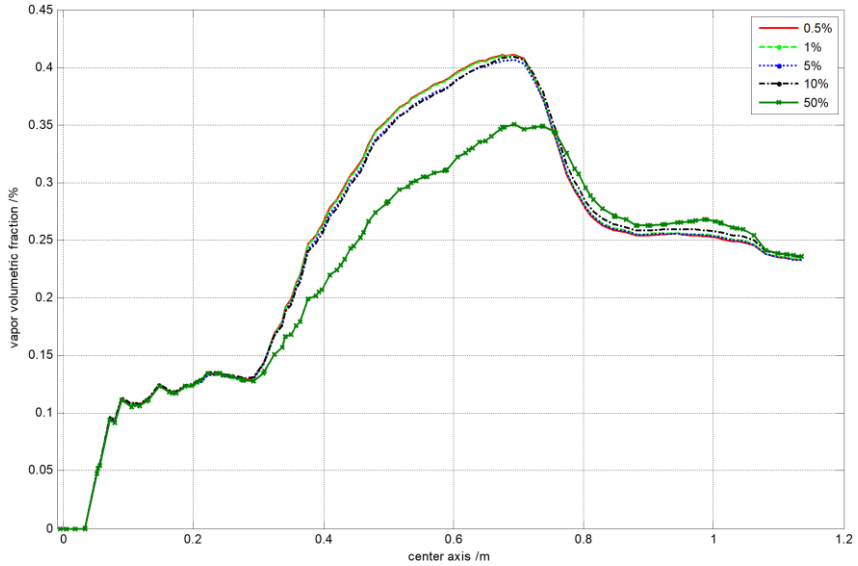

Figure 10. the distribution of relative volume fraction of vapor phase on the center axis.

Conclusion

In concordance with the numerical simulation results, the established model using the two-fluid model and the water evaporation model, and the Reynolds stress model provide a convenient way to study the effects of the different water concentrations in oil. With increasing the water concentration in oil, the turbulent intensity of the oil phase decreases, simultaneously that of the water phase increases, that of vapor phase are practically independents of inlet water concentration of the mixture; the streamline of oil, water, and vapor phase is divided into three layers by the plate column in the canter of the VOF. The separation efficiency has been influenced by the inlet water concentration reaching values between 20.65-22.62 % in the centre axis, while 33.18-42.24% in the plate column; the vapor concentration ranged from 0 - 23.64% in the centre axis, while 0 - 41.02% in the plate column. The relative volume fraction of water concentration decay tending with the water concentration increases.

This concludes that the water concentration is important to influence parameter on the VOF, in consequence, computational fluid dynamics (CFD) techniques can prove useful in understanding important flow mechanisms in the VOF and thus predict its performance. Furthermore, this study demonstrated the challenging task of modelling oil and water separator, and that more work must be done to make the work more complete.

Notation

i the phase

f_i the volume fraction of the i phase

ρ_i phase density[kg/m^3]

u_i, v_i, w_i the velocity of the i phase in x, y, z direction, respectively[m/s]

S_m the mass flow rate per unit volume from water phase to vapor phase[kg/m^3]

μ_i dynamic viscosity of the i phase [Pa.s]

p_i the pressure of the i phase [Pa]

g_x, g_y, g_z the gravitational body force in x, y, z direction, respectively[m/s^2]

$\Psi_{\alpha\beta x}$, $\Psi_{\alpha\beta y}$, $\Psi_{\alpha\beta z}$ momentum transfer induced by interphase mass transfer

F_x, F_y, F_z the total force on one phase due to interaction with other phases[N]

f_o the volume fraction of the oil phase

σ the water/oil surface tension[N/m]

ρ_o oil density [kg/m^3]

ρ_w water density [kg/m^3]

$\overline{\kappa}$ curvature, $\overline{\kappa} = -\left(\nabla \cdot \hat{n}\right)$, the unit normal vector is $\hat{n} = \dfrac{\nabla f_o}{|\nabla f_o|}$

ρ the water/oil mixture density, $\rho = f_o\rho_o + \left(1-\rho_o\right)\rho_w$ [kg/m^3]

$\overline{u_i'}$, $\overline{v_i'}$, $\overline{w_i'}$ the velocity fluctuation average of the i phase in x, y, z direction[m/s]

μ_{it} the turbulent viscosity, $\mu_{it} = \rho C_\mu \dfrac{\kappa^2}{\varepsilon}$

ε the turbulence eddy dissipation

κ the turbulent kinetic energy

P_{xx} stress production[N]

G_{xx} buoyancy production[N]

$C_{\varepsilon 1}$, $C_{\varepsilon 2}$ and $C_{\varepsilon 3}$ Reynolds stress model constants

b_{xy} the Reynolds-stress anisotropy tensor, $b_{xy} = -\dfrac{-\rho_i\,\overline{u_i'v_i'} + \dfrac{2}{3}\rho_i\kappa\delta_{xy}}{2\rho_i\kappa}$

S_{xy} the mean strain rate, $S_{xy} = \dfrac{1}{2}\left(\dfrac{\partial v_i}{\partial x} + \dfrac{\partial u_i}{\partial y}\right)$

Ω_{xz} the mean rate-of-rotation tensor, $\Omega_{xz} = \dfrac{1}{2}\left(\dfrac{\partial u_i}{\partial y} - \dfrac{\partial v_i}{\partial x}\right)$

λ_i the liquid thermal conductivity coefficient[w/m·k]

c_i specific heat capacity [J /(kg·K)]

T_i the droplet temperature[K]

V_{inlet} and V_{outlet} inlet and outlet volumetric fraction

Acknowledgements

This study was funded by National Natural Science Foundation of China (51375516).

References

Abdulredha, M. M., Siti Aslina, H., & Luqman, C. A. (2020). Overview on petroleum emulsions, formation, influence and demulsification treatment techniques. *Arabian Journal of Chemistry, 13*(1), 3403-3428. DOI: https://doi.org/10.1016/j.arabjc.2018.11.014

Abu-Zaid, M. (2004). An experimental study of the evaporation characteristics of emulsified liquid droplets. *Heat & Mass Transfer, 40*(9), 737-741. DOI: https://doi.org/10.1016/0017-9310(88)90271-2

International Energy Agency [IEA]. (2021), *Key World Energy Statistics 2021*, OECD Publishing; Paris. DOI: https://doi.org/10.1787/2ef8cebc-en

Bin, C., & Ge, L. (2022). Effects of particle size and concentration on the pulsation characteristics of transformer oil. *Journal of the National Science Foundation of Sri Lanka, 49*(4), 593-606. DOI: https://doi.org/10.4038/jnsfsr.v49i4.10106

Brackbill, J. U., Kothe, D. B., & Zemach, C. (1992). A continuum method for modeling surface tension. *Journal of Computational Physics, 100*(2), 335-354. DOI: https://doi.org/10.1016/0021-9991(92)90240-Y

Cellini, J. V., Ronghi, M. F., & Geren, J. G. (1988). *Vacuum distillation system* (United States Patent 4770748). Retrieved from https://patentimages.storage.googleapis.com/e7/d6/8d/540c70fa64a759/US4770748.pdf

Clint, J. H., Fletcher, P. D. I., & Todorov, I. T. (1999). Evaporation rates of water from water-in-oil microemulsions. *Physical Chemistry Chemical Physics, 1*(21), 5005-5009. DOI: https://doi.org/10.1039/A906769H

Fletcher, C. A. J. (1988). *Computational Techniques For Fluid Dynamics: Fundamental And General Techniques*. Berlin & New York, Springer-verlag, 72-76.

Gong, H., Li, W., Zhang, X., Peng, Y., Yu, B., & Mou, Y. (2021). Effects of droplet dynamic characteristics on the separation performance of a demulsification and dewatering device coupling electric and centrifugal fields. *Separation and Purification Technology, 257*(1). DOI: https://doi.org/10.1016/j.seppur.2020.117905

Gutiérrez, G., Lobo, A., Benito, J. M., Coca, J., & Pazos, C. (2011). Treatment of a waste oil-in-water emulsion from a copper-rolling process by ultrafiltration and vacuum evaporation. *Journal of Hazardous Materials, 185*(2), 1569-1574. DOI: https://doi.org/10.1016/j.jhazmat.2010.10.088

Haelssig, J. B., Tremblay, A. Y., Thibault, J., & Etemad, S. G. (2010). Direct numerical simulation of interphase heat and mass transfer in multicomponent vapour-liquid flows. *International Journal of Heat & Mass Transfer, 53*(19), 3947-3960. DOI: https://doi.org/10.1016/j.ijheatmasstransfer.2010.05.013

Laza-Knoerr, A., Huang, N., Grossiord, J. L., Couvreur, P., & Gref, R. (2011). Interfacial rheology as a tool to study the potential of cyclodextrin polymers to stabilize oil–water interfaces. *Journal of Inclusion Phenomena & Macrocyclic Chemistry, 69*(3), 475-479. DOI: https://doi.org/10.1007/s10847-010-9805-5

Wang, D., Yang, D., Huang, C., Huang, Y., Yang, D., Zhang, H., ... Zeng, H. (2021). Stabilization mechanism and chemical demulsification of water-in-oil and oil-in-water emulsions in petroleum industry: A review. *Fuel, 286*(1). DOI: https://doi.org/10.1016/j.fuel.2020.119390

Zhao, F., Tian, Z., Yu, Z., Shang, H., Wu, Y., & Zhang, Y. (2020). Research status and analysis of stabilization mechanisms and demulsification methods of heavy oil emulsions. *Energy Science & Engineering, 8*(12), 4158-4177. DOI: https://doi.org/10.1002/ese3.814